Revisiting acoustical gas-mixture separation

Satoshi Sekimoto, Yuji Yamagishi, and Yuki Ueda

Tokyo University of Agriculture and Technology, Koganei, Tokyo 184-8588, Japan

(Dated: 31 January 2024)

This study experimentally investigated acoustically driven gas-mixture separation. Acoustic wave propagation in a narrow tube can induce gas-mixture separation. A binary mixture of helium and argon was used as the gas mixture. The pressure amplitude of the acoustic wave and initial molar fraction of the helium gas were investigated. The obtained experimental data indicated that the molar fraction initially increased with increasing pressure amplitude, whereas the saturated molar fraction did not show a clear dependence on the pressure. Although the degree of separation was smaller with purer helium, gas-mixture separation occurred under all conditions within the experimental range.

I. INTRODUCTION

The propagation of an acoustic wave in a narrow tube results in the formation of a temperature gradient in the radial direction owing to thermal interactions based on the following principle: The compression/expansion of a gas induced by acoustic wave propagation in a tube rises/lowers the temperature of the gas at the center of the tube. By contrast, owing to the relatively large heat capacity of the tube wall, the gas temperature near the tube wall is anchored to that of the tube wall. This acoustically generated temperature gradient can contribute to energy conversion (Biwa *et al.*, 2004), mass transfer (Weltsch *et al.*, 2017), and gas-mixture separation (Spoor and Swift, 2000).

This study focuses on the acoustical gas-mixture separation that was investigated in detail by a research group at Los Alamos National Laboratory(LANL). The group briefly explained the mechanism of acoustic gas separation and derived a theory (Swift and Spoor, 1999), (Geller and Swift, 2002a), (Geller and Swift, 2009). This theory indicates that the separation depends on the characteristics of the acoustic wave, such as the amplitude of the pressure or velocity oscillations and the phase difference between them. It also depends on the geometry of the tube, such as the tube radius. The LANL group conducted experiments using a helium-argon gas mixture and quantitatively confirmed these results. However, few reports except those from the LANL group are available. Hence, in this study, we revisit acoustical gas-mixture separation experimentally and focus on two important parameters. The first parameter is the amplitude of the acoustic waves. In theory, increasing the amplitude is essential for separation. Therefore, we used a tube with a length comparable to the

wavelength of a sound wave to utilize acoustic resonance. This enabled an increase in the pressure amplitude to approximately 9 kPa in this study, which was 9% of the time-averaged pressure of the gas mixture charged in our experimental setup and was 4.5 times larger than that of the experiments by the LANL group (Spoor and Swift, 2000). The second parameter is the initial molar fraction of the helium and argon gases;

$$n_{He} = \frac{N_{He}}{N_{Ar} + N_{He}}, \tag{1}$$

where N_{He} and N_{Ar} are the mole numbers of the helium and argon gases in the experimental setup, respectively. Although increasing the separation rate in one separation step is essential, multi-stage separation is also considered as an effective method for obtaining higher helium concentrations. Therefore, the dependence of the effect of acoustical gas-mixture separation on n_{He} is important.

The paper is organized as follows. Section II describes the experimental setup, procedures, and measurement methods used to determine the molar fraction of the gas mixture. Experimental results focusing on the time dependence of the molar fraction, effects of the pressure amplitude, and initial molar fraction are shown and discussed in Section III. Finally, the conclusions are presented in Section IV.

II. EXPERIMENTAL SETUP AND PROCEDURE

A. Setup

The experimental apparatus comprised a speaker unit and three types of tubes, as shown in Fig. 1. The speaker unit incorporated a nominal 6.5”/160 mm diameter moving-coil

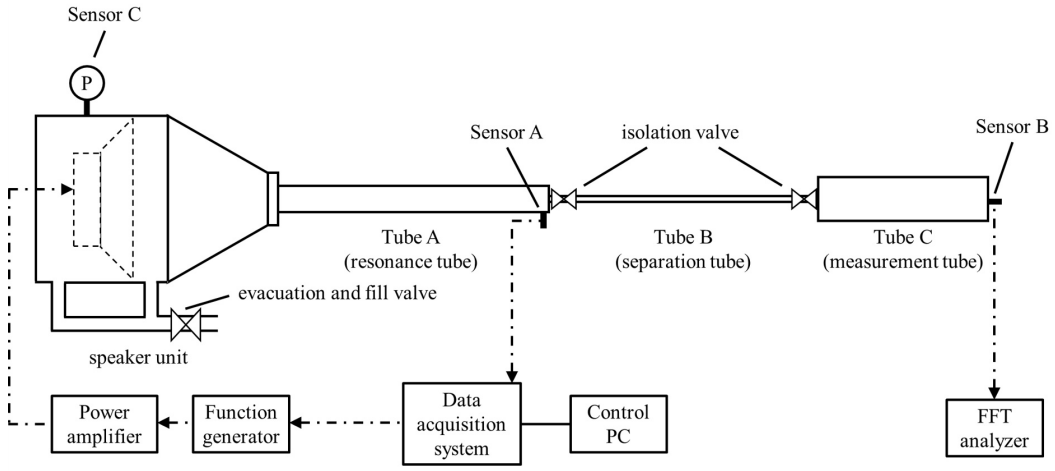

FIG. 1. Schematic of the experimental apparatus. Note that the dimensional ratio of each part (for example, the diameter/length ratio) differs from that of the actual apparatus.

electrodynamic loudspeaker with an effective piston area of 133 cm^2 (FW168HS, Fostex Ltd.) and was connected to Tube A by a tapered part. The volume between the diaphragm and Tube A was 1.09×10^6 mm^3, and the volume behind the diaphragm was 1.59×10^6 mm^3. The input sinusoidal waveform was generated using a function generator (Agilent Technologies 33210A) and amplified using a 350 W stereo audio power amplifier (P2500S, Yamaha Corporation). The inner radius and length of Tube A were 11.5 mm and 2.0 m, respectively. The other end of Tube A was closed using a rigid plate with a small hole. A copper tube, referred to as Tube B, was connected to the hole and had the same diameter as the outer diameter of Tube B. Because the inner radius of the tube was the narrowest in the apparatus, the gas-mixture separation was expected to occur mainly in this part. The inner radius and length of Tube B were 2.4 mm and 1.86 m, respectively. Tube C was connected to the other end of Tube B. The inner radius and length of Tube C were 18.9

mm and 0.148 m, respectively. The apparatus had two types of valves: one (evacuation and fill valve) was used to separate the gas inside and outside, and the other was used to isolate Tube C. Two types of sensors were mounted on the apparatus. Sensors A and B (PD104, Jtect Ltd.) were used to measure the acoustic pressure amplitude at the ends of Tubes A and C, respectively. These sensors were piezoresistive, and one side of the diffusion-type gauge was opened to the atmosphere. Both steady and acoustic pressures were measured, and the amplitude corresponding to the driving frequency was extracted. Sensor C (GP-M025, Keyence Corporation) was mounted on the speaker unit to monitor the internal mean pressure. The signals from Sensors B and C were analyzed using a fast Fourier transform analyzer (DS-3000, Onosokki Ltd.). As described in the next section, the sinusoidal input waveform to the speaker unit was adjusted according to the progress of separation. Therefore, the function generator and Sensor A were connected to a data acquisition system (USB-6363 and BNC-2120, National Instruments Corporation), and the amplitude and frequency of the input waveform were feedback-controlled.

The working gas was a binary mixture of helium and argon. The temperature of the experimental apparatus was controlled to room temperature (approximately 20°C) using a normal air conditioner. The room temperature fluctuated by approximately ±1 °C during the experiment. Note that throughout the experiment, the local temperature in the apparatus was subject to change owing to the thermoacoustic effect.

B. Procedure

Five preliminary steps were performed before the experiments. First, the gas in the experimental setup was vacuumed from the evacuation-and-fill valve under the condition that all valves were open, and then the two isolation valves were closed. Second, helium and argon gases were injected sequentially into the apparatus. The amount of injected gas was monitored using Sensor C. The time-averaged pressure inside the apparatus p_m was approximately 100 kPa. The two gases did not mix immediately after injection and were unevenly distributed in the tube. Third, an acoustic wave was input from the speaker to forcibly mix the two gases in Tube A. The progress of the binary gas mixing was checked using the first resonance frequency in Tube A. Preliminary experiments showed that the resonance frequency in Tube A corresponded to the molecular weight of the initially injected gas and gradually approached the frequency corresponding to the average molecular weight of the mixed gas. In this procedure, the first-resonance-frequency sound wave with a pressure amplitude of 3.0 kPa was applied. The driving (resonance) frequency was adjusted and observed once every 3 min during the forcible mixing. When the frequency change became less than 0.25, the sound wave input was stopped, and the resonant frequency continued to be measured once every 3 min. Figure 2 shows the time dependence of the resonance frequency in Tube A. The mixing procedure required approximately 1 h. After mixing, the experimental apparatus was allowed to stand for approximately one day. Fourth, the two isolation valves were opened, and the mixed gas was introduced into Tubes B and C. Fifth, the molar fraction in Tube C, $n_{C,He}$, was measured according to the method described in

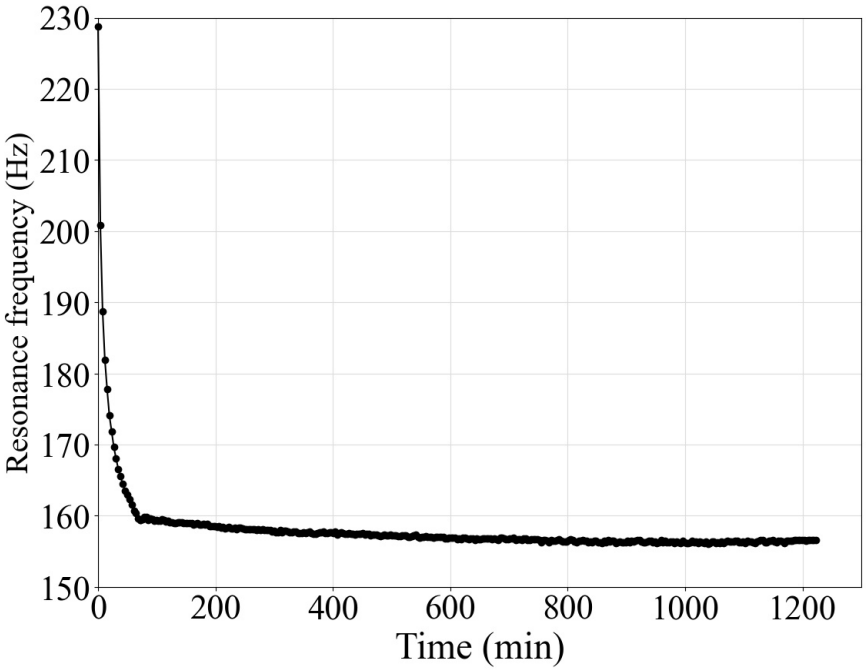

FIG. 2. Time dependence of the resonance frequency in Tube A. The depicted case used the gas mixture with a helium initial molar fraction of 50.0 %.

the next subsection and compared with the value estimated from the amounts of the two gases injected in the second step. If the two values were consistent, the measured $n_{C,He}$ was considered as the initial molar fraction $n_{0,He}$.

After the preparations, an acoustic wave with the second resonance frequency f was applied under the condition that both isolation valves were opened, and gas separation was initiated. Although we do not discuss the effect of the mode of the resonance frequency on the gas-separation capability in this study, preliminary experiments showed that an acoustic wave with the second resonance frequency had a better gas-separation capability than that with the first resonance frequency. Therefore, we focused on the second resonance. Because the resonance frequency f gradually changed as the separation progressed, the

driving frequency of the speaker was adjusted. Here, the resonance frequency is defined as the frequency that generates the maximum pressure amplitude at Sensor A with the same input voltage amplitude to the loudspeaker. The resonance frequency was determined by sweeping the driving frequency. The input voltage amplitude to the speaker was adjusted using the determined resonance frequency such that the pressure amplitude p_A at Sensor A was at the target value. The frequency and voltage amplitude were adjusted every 10 min. Note that the two valves were always open except during the measurement of the molar fraction $n_{C,He}$ in Tube C described in the next subsection.

C. Measurement method of molar fraction

The first resonance frequency f_{Ctube} in the cylindrical tube corresponds to $a_0/2l$, where a_0 and l are the adiabatic sound speed and cavity length, respectively, when the valve between Tube B and Tube C is closed. Using the averaged molar weight m_{avg} of the gas, a_0 is expressed as $\gamma \mathrm{R} T_m/m_{avg}$, where γ is the specific heat ratio, R is the universal gas constant, and T_m is the time-averaged absolute temperature. Using these two equations, the following equation is derived:

$$m_{avg} = \gamma \mathrm{R} T_m \left(\frac{1}{2l f_{Ctube}} \right)^2 \tag{2}$$

In this study, m_{avg} was expressed in another form as follows:

$$m_{avg} = m_{He} n_{He} + m_{Ar}(1 - n_{He}), \tag{3}$$

where m_{He} and m_{Ar} are the molar weights of helium and argon, respectively. Transforming these equations yields the following equation for the helium molar fraction:

$$n_{He} = \frac{m_{Ar} - m_{avg}}{m_{Ar} - m_{He}} \tag{4}$$

Note that the thermal boundary layer thickness calculated using equation (A4) in Appendix has a maximum value of 0.77% at approximately $n_{He} = 0.8$. This value indicates that the boundary layer correction can be neglected in Tube C.

The measurement procedure for n_{He} is as follows: First, both isolation valves were closed. Second, the gas column inside Tube C was excited using an impact hammer, and a sensor signal was obtained. Third, the signal was analyzed using the fast Fourier transform analyzer, and the first resonance frequency of the gas column in Tube C was obtained. Finally, the molar fraction in Tube C $n_{C,He}$ was estimated by substituting the obtained resonance frequency into Eqs. (2) and (4). The error in measuring the molecular weight using this method was confirmed to be approximately 0.58 for air, 0.67 for pure helium, and 0.33 for pure argon. This result indicates that the current method can measure the molecular weight with an error of approximately 0.7 regardless of the separation state. This error in the molecular weight corresponds to an approximately 1.9% molar fraction error for the He-Ar gas mixture.

III. RESULTS AND DISCUSSIONS

A. Time dependence of molar fraction

In this subsection, one of the experimental results we obtained is taken as an example to show the time dependence of gas separation. The initial molar fraction $n_{0,He}$ was 0.50, and the pressure amplitude p_A was set at 3.0 kPa. The driving frequency corresponding to the second mode was approximately 159 Hz at the beginning of the experiment. The values of p_A and $n_{0,He}$ are similar to those in the experimental study by the LANL group (Spoor and Swift, 2000), although the frequency in this study is much higher than that in their study. The sound wave with this frequency in the current-mixed gas had a wavelength comparable to that of Tube B.

Figure 3 displays the time dependence of $n_{C,He}$. First, the data near $t = 0$ is considered. Figure 3 shows that $n_{C,He}$ near $t = 0$ rapidly increases. Here, the experimental rate of increase $n_{C,He}$ is defined as

$$\dot{n}_{C,He}(t_i) = \frac{n_{C,He,i+1} - n_{C,He,i}}{t_{i+1} - t_i}, \tag{5}$$

where i is the index of the acquired data. The molar flow into Tube C can be calculated using $\dot{n}_{C,He}$ and the volume of Tube C, V_C, as

$$\dot{N}_{He}(t_i) = \dot{n}_{C,He}(t_i) \times \frac{p_m V_C}{R T_m(t_i)}, \tag{6}$$

Processing data shown in Fig. 3, $\dot{N}_{He}(0)$ of this experiment were determined to be 3.0×10^{-8} mol/s, which is comparable to the value reported by the LANL group (Spoor and Swift, 2000).

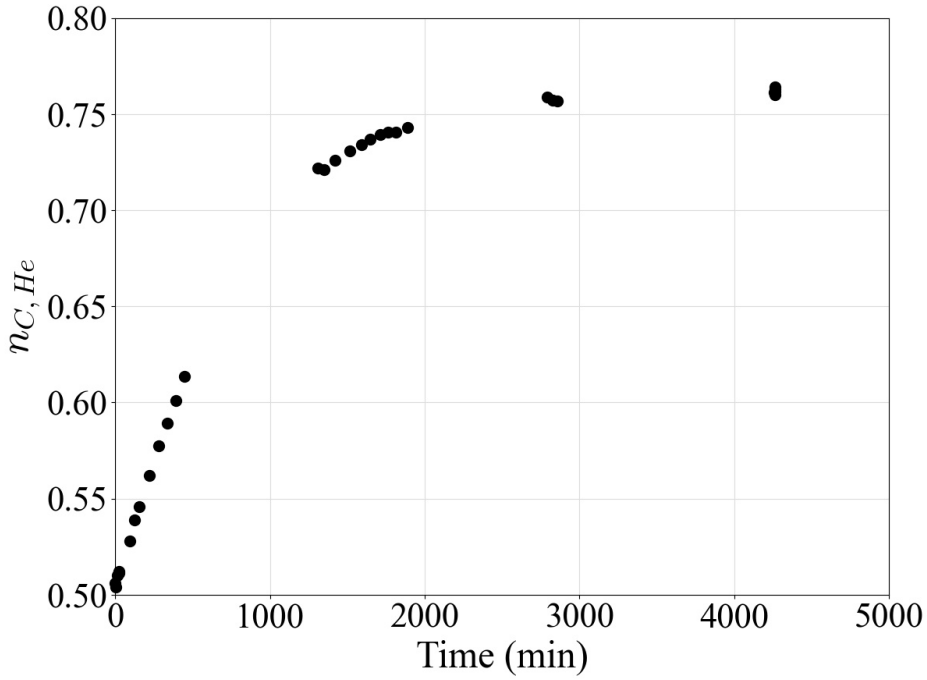

FIG. 3. Time dependence of the mole fraction $n_{C,He}$. The gas-separation experiment was conducted under the condition that the initial molar fraction $n_{0,He}$ was 0.50, and the pressure amplitude p_A was 3.0 kPa.

Next, we focused on the data under saturated conditions. Figure 3 shows that the saturated $n_{C,He}$ is 76.0%. Now, there are two common boundary conditions throughout the experiment: the velocity at the end of Tube C was zero, and the pressure amplitude at the beginning of Tube B was set to the target value (3.0 kPa in this case). In the saturated condition, the driving frequency was 159.2 Hz, and the molar fraction at the end of Tube C was 76.0 % under the assumption that the molar fraction in Tube C was constant. Under these conditions, the acoustic and molar-fraction distributions in the saturated condition can be estimated as shown in Fig. 4. The commonly used thermoacoustic software DeltaEC was used for this calculation (Ward *et al.*).

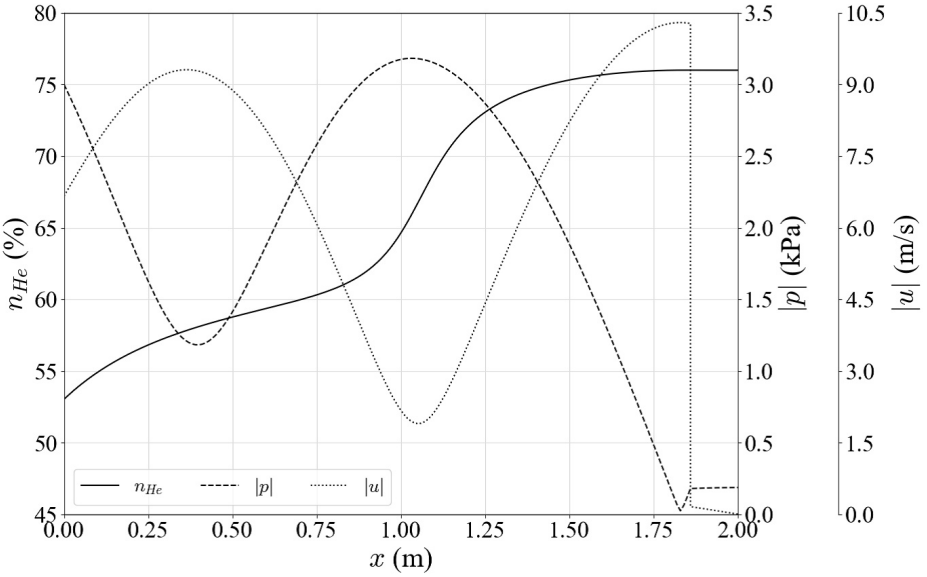

FIG. 4. Estimated acoustic and molar-fraction distributions in Tube B and C at the saturated condition. The commonly used thermoacoustic software DeltaEC was used for this calculation (Ward *et al.*).

Figure 4 shows a notable molar-fraction gradient in Tube B, while the molar fraction is almost constant in Tube C (as expected). The molar fraction in Tube B does not vary linearly in the axial direction, and the gradient is locally large near the antinode of the pressure amplitude (node of the velocity amplitude). The estimated molar fractions at the beginning and end of Tube B are 53.0 % and 76.0 %, respectively. Therefore, the gradient of n_{He} along Tube B is 12.4(% /m), which is also comparable to the data of the LANL group (Spoor and Swift, 2000). Therefore, a tube with a length comparable to the acoustic wavelength can contribute to acoustic gas-mixture separation. These results motivate us to perform acoustical gas-mixture separation using a thermoacoustic engine that has no moving parts and can be powered by an external heat source.

The increased number of molecules in Tube C originates from the space to the left of Tube B, which includes Tube A. Assuming that the molar fraction is constant in the spaces to the left of Tube B and also in Tube C, the decrease in the molar concentration in Tube A is estimated to be approximately 1.2% based on the volume ratio and the increase in the molar fraction by 26 % in Tube C. Surprisingly, however, the calculation result displayed in Fig. 4 shows that the molar fraction at the beginning of Tube B (i.e., the end of Tube A) increases from the initial value of 50 %. This suggests that a molar-fraction distribution occurs in Tube A, even though the tube radius is larger than Tube B.

If appropriate boundary conditions in the final state are available, the acoustic and molar-fraction fields in the final state can be determined in advance. However, to the best of the author's knowledge, it is impossible to determine the appropriate boundary conditions for the final state in advance, which implies that the final separation state cannot be predicted. This is caused by the change in the molar-fraction distribution during the gas-mixture separation. Overcoming this issue requires the knowledge of the molar fraction distribution after the start of separation; namely, it requires a time-evolution solver.

B. Effect of pressure amplitude

Because the acoustic wave was driven by the resonance frequency in this experiment, p_A can easily be set to a large value. Acoustical gas-mixture separation was performed with $p_A = 1.5$, 3, 6, and 9 kPa. Here, we focus on two quantities: $\dot{N}_{He}$ near $t = 0$ and Δn_{He}.

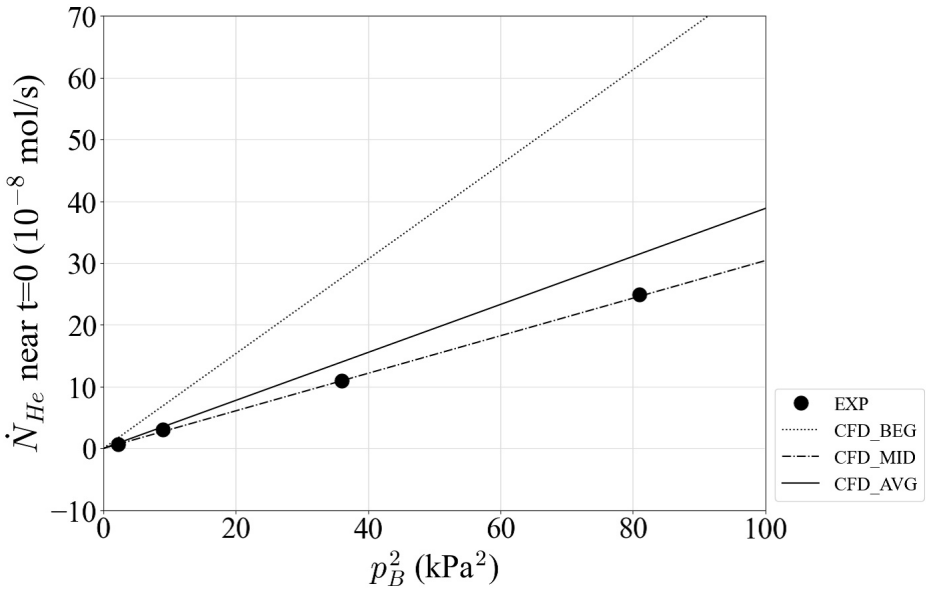

FIG. 5. Pressure-amplitude dependence of $\dot{N}_{He}$ near $t = 0$. Note that the values are plotted as a function of p_B^2. Black-filled circles display the values estimated from the experimental results by Eq. (5) and (6). The calculated $\dot{N}_{He}$ at the beginning (CFD_BEG), midpoint (CFD_MID), and the overall average (CFD_AVG) of Tube B at $t = 0$ are plotted as a function of the pressure amplitude with lines.

Figure 5 shows $\dot{N}_{He}$ near $t = 0$ as a function of p_A^2. The black circles display the experimental results, which indicate that $\dot{N}_{He}$ increases linearly with p_A^2 within the experimental range.

Geller and Swift derived the theory and equation for $\dot{N}_{He}$ in (Geller and Swift, 2002a) and arranged it as Eq. (A1) in (Geller and Swift, 2004). In the initial state (before gas separation was commenced), there was no molar fraction gradient in the apparatus, and dn_{He}/dx could be considered as zero everywhere. In addition, because this experiment was conducted in a sealed system, the total molar flux was zero, that is, $\dot{N}_{He} = -\dot{N}_{Ar}$ at all

209 locations, where $\dot{N}_{Ar}$ indicates the molar flux of argon. Therefore, the equation can be
210 expressed as:

$$\frac{\dot{N}_{0,He}}{A_{gas}} = -\frac{\delta_\alpha}{4r_h}\frac{\gamma-1}{\gamma}\frac{k_T}{R_{univ}T_m}|p||u|[F_{trav}\cos\theta + F_{stand}\sin\theta] \tag{7}$$

211 where A_{gas} denotes the cross-sectional area of a flow channel, δ_α denotes the thermal bound-
212 ary layer thickness, r_h denotes the tube radius, γ denotes the specific heat ratio, k_T denotes
213 the thermal diffusion ratio which is proportional to the driving force of the Soret effect
214 (reviewed in detail in (Platten, 2006) and (Rahman and Saghir, 2014)), R_{univ} denotes the
215 universal gas constant, and θ denotes the phase difference at which p leads u. The definitions
216 of F_{trav}, F_{stand}, and related values are provided in the Appendix. All the values except p, u,
217 and θ depend only on the current molar fraction. Therefore, if the distributions of p and
218 u are obtained, the $\dot{N}_{0,He}$ distribution in the initial state can be calculated. We estimated
219 the p and u distributions based on the linear acoustic theory (Swift, 2003), including the
220 evolution of u (Geller and Swift, 2002b) modified for gas-separation calculations and the
221 effect of a minor loss (Ueda *et al.*, 2020) occurring at the junction of Tubes B and C. Figure
222 6 shows the calculated distributions of $\dot{N}_{He}$ at $t = 0$ as a function of the axial position. The
223 plotted cases correspond to the experimental conditions. The magnitude is the largest near
224 the beginning of the tube and decreases toward the end although there is a local flat dis-
225 tribution. The basic distribution shape remains almost the same regardless of the pressure
226 amplitude in the calculations according to the linear thermoacoustic theory.

228 The numerically calculated $\dot{N}_{He}$ of the beginning (CFD_BEG), midpoint (CFD_MID, x
229 = 0.93 m), and overall average (CFD_AVG) of Tube B at $t = 0$ are plotted as a function
230 of the pressure amplitude with lines in Fig. 5. The experimental and numerical results

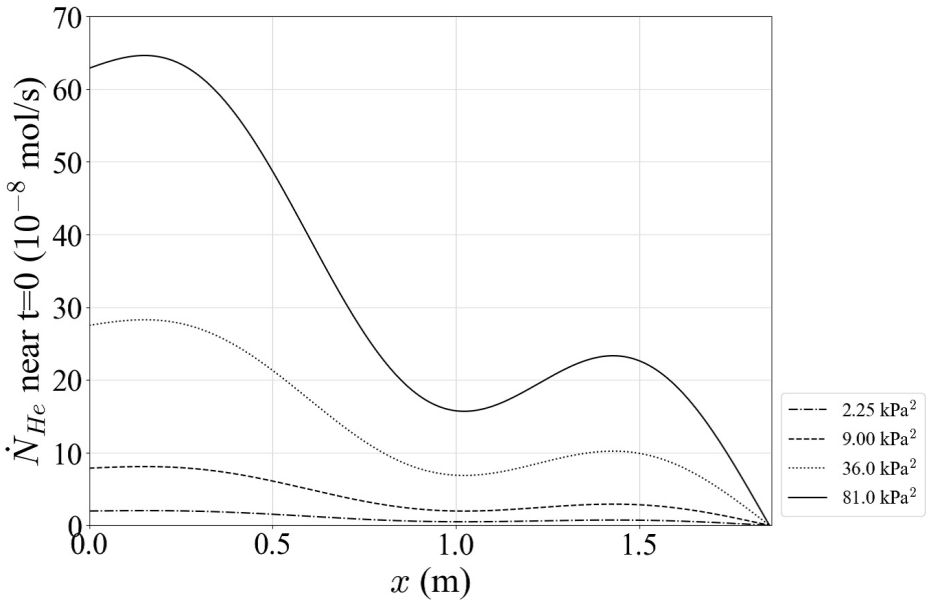

FIG. 6. Distributions of $\dot{N}_{He}$ at $t = 0$. The plotted cases correspond to the experimental conditions in Fig. 5.

qualitatively show the same trend: $\dot{N}_{He}$ increases linearly with p_b^2. Although the result of the midpoint of Tube B matches well with that of the experiments, we consider this to be coincidental because the $\dot{N}_{He}$ distribution can change depending on the tube length and separation progress. In addition, the experimental results represent the average value of the change over 10 min from the start, whereas the calculations represent the local value at the initial state. The following two points are important in this plot. The first is that the experimentally obtained results are similar to the order of those obtained by calculations. The second is that $\dot{N}_{He}$ changes linearly with respect to the pressure amplitude in the experiment and calculation.

Figure 7 displays Δn_{He} as a function of p_B^2. This figure shows that Δn_{He} increases with increasing p_B^2 when p_B^2 is less than or equal to $(3\ \mathrm{kPa})^2$. In contrast, when p_B^2 is greater than

or equal to $(6\ \text{kPa})^2$, Δn_{He} decreases. Note that the theoretical Δn_{He} is difficult to obtain because the position-dependent n_{He} in the setup changes as the gas separation progresses and is not constant along Tube B. Based on the experimental results, an excessively large pressure amplitude is not suitable for acoustical gas-mixture separation, and the appropriate pressure amplitude to obtain a larger Δn_{He} is 6% of p_m (6 kPa) in this experiment. The LANL group observed a decrease in Δn_{He} and concluded that this was due to mixing by acoustic streaming (Geller and Swift, 2002a). Another possibility is acoustic turbulence. As described in the introduction, the generation of a temperature gradient in the radial direction due to the compression/expansion of gas and the movement of gas molecules due to the Soret effect are very important in gas-mixture separation. In the range of the conventional linear thermoacoustic theory, the flow in the tube is assumed to be laminar, and there is no flow in the radial direction. Under these conditions, the Soret effect is the only driving force for gas-molecule movement in the radial direction. However, acoustic waves with a very large amplitude cause acoustic turbulence and the "laminar flow" assumption cannot be applied. Turbulent flow causes a radial-direction flow, which may cause gas-particle movement due to convection and lead to the cancellation of the biased gas-molecule distribution due to the Soret effect. Ohmi et al. summarized the regimes of oscillating flow by the square root of the dimensionless frequency $\omega' = r^2\omega/\nu$ and acoustic Reynolds number Re_{os} (Ohmi and Iguchi, 1982), where ω denotes the angular frequency of an acoustic wave, and ν denotes the kinematic viscosity. The acoustic Reynolds number is defined as follows:

$$\text{Re}_{os} = \frac{2r|u|}{\nu} \tag{8}$$

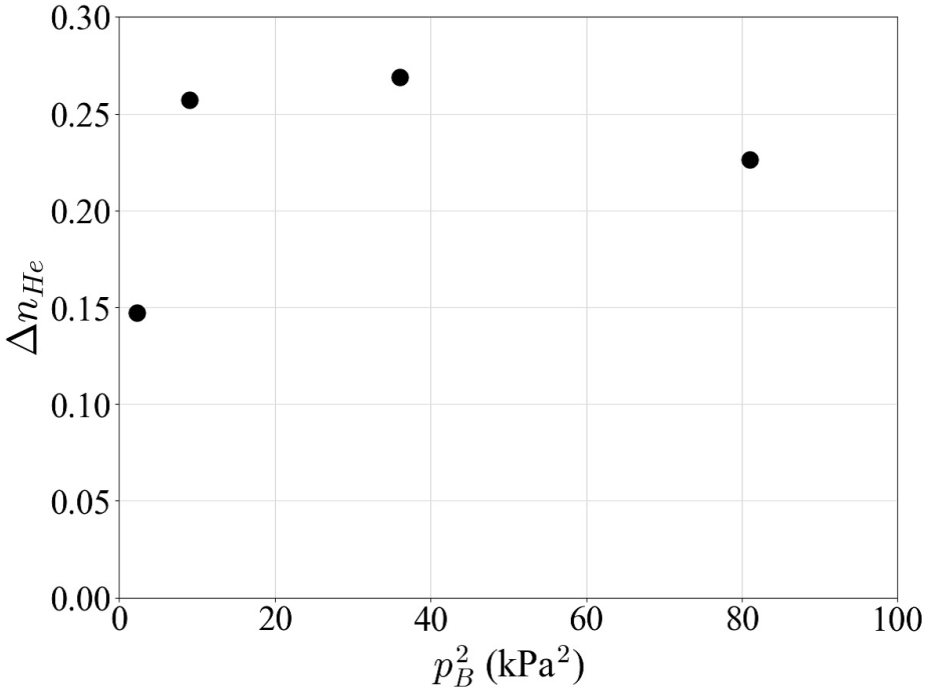

FIG. 7. Pressure-amplitude dependence of Δn_{He} as a function of p_B^2

Under the condition that the pressure amplitude is 9 kPa in Fig. 7, ω' and Re_{os} are 15.2 and 4.22×10^3, respectively. This condition falls in the transient region between the laminar and turbulent regions. Therefore, there is a possibility that the effect of acoustic turbulence has appeared to some extent, leading to a decrease in the gas-mixture separation under this condition.

C. Effect of initial molar fraction

As demonstrated in Section III B, there is a limitation to how much $n_{C,He}$ can be increased by increasing p_B. Hence, to obtain high-purity helium gas from a He-Ar mixture, we assume a different method: multi-stage gas-mixture separation. Considering a two-stage

gas separation as an example, the first-stage process generates a middle n_{He} mixture from a low one, and then the second-stage process generates a higher n_{He} mixture from the middle one. Because this method considers gas-mixture separation at multiple mole fractions, the effects of $n_{0,He}$ on $\dot{N}_{He}$ and Δn_{He} are significant. Hence, the initial molar fraction $n_{0,He}$ were set to 0.28, 0.70, and 0.90, respectively, and $\dot{n}_{C,He}$ near $t = 0$ and Δn_{He} were measured under saturated conditions. During the experiments, p_B was maintained at 6 kPa, and the driving frequency was adjusted to the second resonance frequency. The frequency changed according to the value of $n_{0,He}$.

Figure 8 shows $\dot{N}_{He}$ near $t = 0$ as a function of $n_{0,He}$. The dashed line is calculated in the same manner as shown in Fig. 5. The experimental data at $n_{0,He} = 0.50$ are the same as those presented in Section III B. The figure shows that the experimental values of $\dot{N}_{He}$ are of similar magnitudes, indicating that the acoustic gas-mixture separation can work in a wide range of $n_{0,He}$. Moreover, the experimental and computational results exhibit a maximum at approximately $n_{0,He} = 0.70$.

We consider the dependence of the thermal diffusion ratio k_T on n_{He} in Eq. (7) as the main reason. Atkins et al. experimentally investigated k_T and proposed an approximate formula (Atkins *et al.*, 1939). Figure 9 shows a plot of k_T as a function of n_{He} along a solid line, where k_T is calculated using the approximate formula of the $Helium - argon$ section of the above reference. This figure indicates that k_T is zero at $n_{He} = 0.0$ and 1.0 and has a clear peak at approximately $n_{He} = 0.65$. In contrast, although the products of the other values, except for k_T in Eq. (7), depend on n_{He}, the difference is approximately twice as

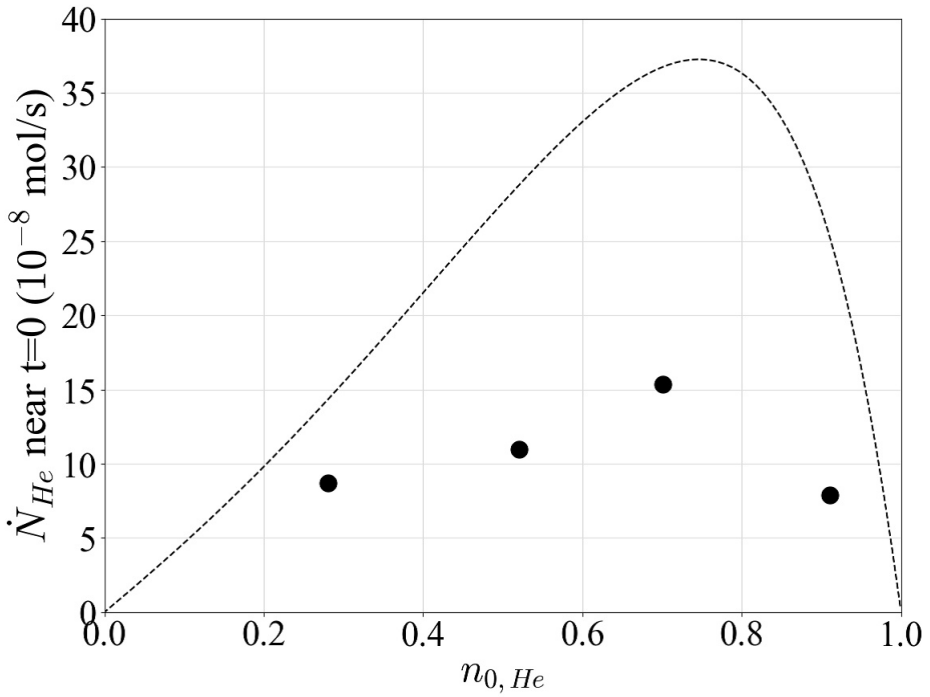

FIG. 8. Initial-molar-fraction $n_{0,He}$ dependence of the $\dot{N}_{He}$ near $t = 0$. Black-filled circles and a dashed line are calculated in the same manner as shown in Fig. 5.

large. Therefore, it can be concluded that k_T mainly depends on the initial molar fraction, as shown in Fig. 8.

Figure 10 shows Δn_{He} as a function of $n_{0,He}$. The black circles display the experimental results, and the solid line is the upper limit of Δn_{He} (e.g. when $n_{0,He}$ is 0.7, the upper limit of Δn_{He} is 0.3). This figure shows that Δn_{He} is 0.2 when $n_{0,He}$ is 0.70, implying that $n_{C,He}$ under the saturated condition is 0.90, and $n_{C,He} = 0.98$ can be obtained from the gas mixture of $n_{0,He} = 0.90$. Although the degree of separation was smaller with purer helium, gas-mixture separation occurred under all conditions within the experimental range. The

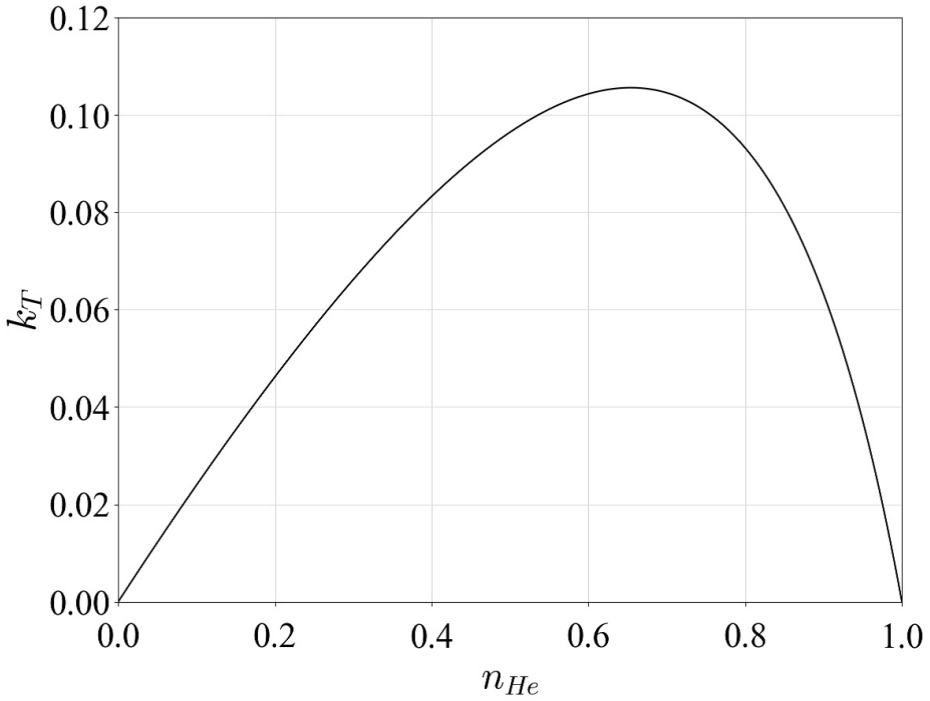

FIG. 9. Molar-fraction n_{He} dependence of the thermal diffusion ratio k_T from (Atkins *et al.*, 1939)

results indicate that a multi-stage gas-mixture separation system can be used to obtain purer gas.

IV. SUMMARY AND CONCLUSIONS

This study experimentally investigated acoustical gas-mixture (helium and argon) separation. We focused on two important parameters for the gas-mixture separation: the pressure amplitude of the acoustic wave and the initial molar fraction. The results showed that our apparatus could induce gas-mixture separation. A gradual increase in the molar fraction in the measurement tube was observed. Although the experimental conditions were not the same as those in a previous study by the LANL group, the initial molar flux and final

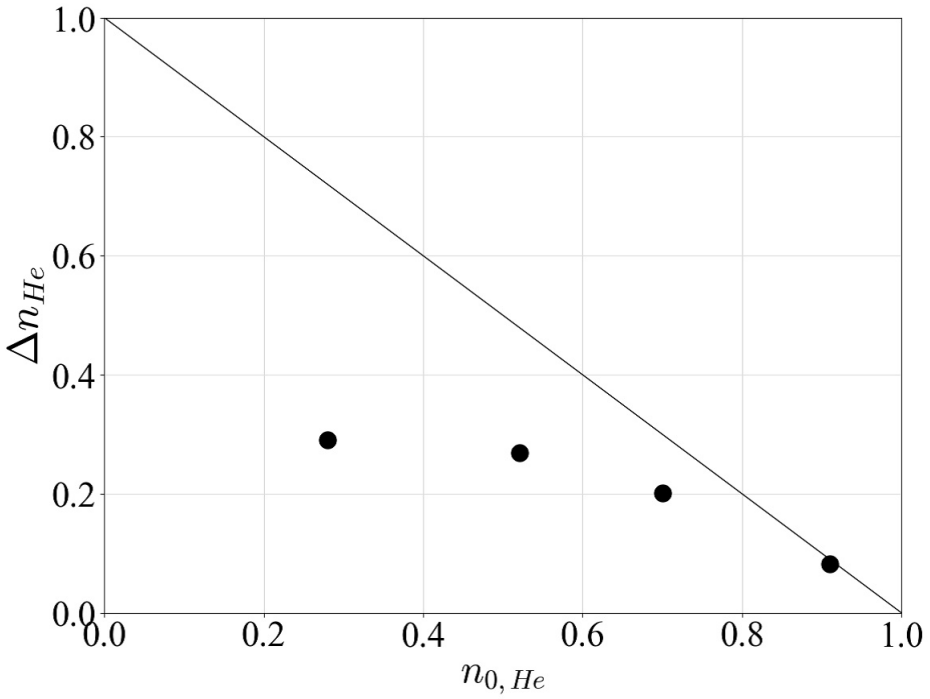

FIG. 10. Initial-molar-fraction $n_{0,He}$ dependence on Δn_{He}. A solid line shows the upper limit of Δn_{He}.

molar-fraction gradient of our experiment were confirmed to be comparable. Increasing the pressure amplitude increased the initial molar flux. However, the degree of final separation had a peak value, and a larger pressure amplitude did not always result in better separation. The initial molar flux depended on the initial molar flux and peaks at an initial molar fraction of approximately 0.7. This suggests that the thermal diffusion ratio significantly affected the initial molar flux. Although the degree of separation was smaller with purer helium, gas-mixture separation occurred under all conditions within the experimental range. This result indicates that a multi-stage gas-mixture separation system can be used to obtain purer gas.

ACKNOWLEDGMENTS

This research was funded by the Japan Society for the Promotion of Science (JSPS) through Grants-in-Aid for Scientific Research (KAKENHI) grant number JP22H01966. The authors thank Y. Ogita, K. Akisue, and K. Watanabe for their contributions to this study.

AUTHOR DECLARATIONS

Conflict of Interest

The authors declare no conflict of interest.

Data Availability

Data are available from the authors upon request.

APPENDIX: CALCULATION OF F_{TRAV} AND F_{STAND}

F_{trav} and F_{stand} are defined as follows (Geller and Swift, 2004):

$$F_{trav} = -\frac{2r_h}{\delta_\alpha}\mathrm{Re}\left[\frac{G}{1-\tilde{\chi_\nu}}\right] \tag{A1}$$

$$F_{stand} = \frac{2r_h}{\delta_\alpha}\mathrm{Im}\left[\frac{G}{1-\tilde{\chi_\nu}}\right] \tag{A2}$$

$\chi_j(j = \nu, \alpha D, D\alpha)$ is a complex function for function for a circular tube flow channel defined as follows:

$$\chi_j = \frac{2J_1(Y_j)}{Y_j\ J_0(Y_j)} \tag{A3}$$

where

$$Y_j = \frac{(i-1)r}{\delta_j} \tag{A4}$$

and J_α, r, and $\delta_j (j = \nu, \alpha, \alpha D, D\alpha)$ are the Bessel functions of the α-th kind, the radius of the tube, and the boundary layer thickness, respectively. Each boundary layer thickness is defined as follows:

$$\delta_\nu = \sqrt{\frac{2\nu}{\omega}} \tag{A5}$$

$$\delta_\alpha = \sqrt{\frac{2\alpha}{\omega}} \tag{A6}$$

$$\delta_{\alpha D}^2 = \frac{1}{2}{\delta_\alpha}^2[1 + (1+\varepsilon)/L + \sqrt{[1+(1+\varepsilon)/L]^2 - 4/L}] \tag{A7}$$

$$\delta_{D\alpha}^2 = \frac{1}{2}{\delta_\alpha}^2[1 + (1+\varepsilon)/L - \sqrt{[1+(1+\varepsilon)/L]^2 - 4/L}] \tag{A8}$$

where

$$\varepsilon = \frac{\gamma - 1}{\gamma}\frac{k_T^2}{n_H(1-n_H)} \tag{A9}$$

$$L = \frac{\alpha}{D_{12}} \tag{A10}$$

and ν, α, k_T, n_H, and D_{12} are the kinematic viscosity, thermal diffusivity, thermal diffusion ratio, molar fraction of the heavier component, and mutual diffusion coefficient, respectively. G and related values are defined as follows:

$$S = \left(\frac{\delta_\alpha^2}{\delta_{D\alpha}^2} - 1\right)\chi_{D\alpha} - \left(\frac{\delta_\alpha^2}{\delta_{\alpha D}^2} - 1\right)\chi_{\alpha D} \tag{A11}$$

$$Q = \frac{\delta_{\alpha D}^2 - \delta_{D\alpha}^2}{\delta_\alpha^2} \tag{A12}$$

$$M = (1+\sigma)(1+\sigma L) + \varepsilon\sigma \tag{A13}$$

$$G = \frac{\sigma L Q}{MS}\chi_{\alpha D}\chi_{D\alpha} + \frac{\tilde{\chi_\nu}}{S}\left(\frac{\chi_{\alpha D}}{1+\delta_\nu^2/\delta_{D\alpha}^2} - \frac{\chi_{D\alpha}}{1+\delta_\nu^2/\delta_{\alpha D}^2}\right) \tag{A14}$$

where σ denotes the Prandtl number.

Atkins, B., Bastick, R., and Ibbs, T. (**1939**). "Thermal Diffusion in Mixtures of the Inert Gases," Proceedings of the Royal Society of London. Series A. Mathematical and Physical Sciences **172**(948), 142–158.

Biwa, T., Tashiro, Y., Mizutani, U., Kozuka, M., and Yazaki, T. (**2004**). "Experimental Demonstration of Thermoacoustic Energy Conversion in a Resonator," Physical Review E **69**(6), 066304.

Geller, D., and Swift, G. (**2002**a). "Saturation of Thermoacoustic Mixture Separation," The Journal of the Acoustical Society of America **111**(4), 1675–1684.

Geller, D., and Swift, G. (**2002**b). "Thermodynamic Efficiency of Thermoacoustic Mixture Separation," The Journal of the Acoustical Society of America **112**(2), 504–510.

Geller, D., and Swift, G. (**2004**). "Thermoacoustic Enrichment of the Isotopes of Neon," The Journal of the Acoustical Society of America **115**(5), 2059–2070.

Geller, D., and Swift, G. (**2009**). "Thermoacoustic Mixture Separation with an Axial Temperature Gradient," The Journal of the Acoustical Society of America **125**(5), 2937–2945.

Ohmi, M., and Iguchi, M. (**1982**). "Critical Reynolds Number in an Oscillating Pipe Flow," Bulletin of Japan Society of Mechanical Engineers **25**(200), 165–172.

Platten, J. K. (**2006**). "The Soret Effect: a Review of Recent Experimental Results," The Journal of Applied Mechanics **73**(5), 5–15.

Rahman, M., and Saghir, M. (**2014**). "Thermodiffusion or Soret Effect: Historical Review," International Journal of Heat and Mass Transfer **73**, 693–705.

Spoor, P., and Swift, G. (**2000**). "Thermoacoustic Separation of a He-Ar Mixture," Physical review letters **85**(8), 1646.

Swift, G., and Spoor, P. (**1999**). "Thermal Diffusion and Mixture Separation in the Acoustic Boundary Layer," The Journal of the Acoustical Society of America **106**(4), 1794–1800.

Swift, G. W. (**2003**). *Thermoacoustics: A Unifying Perspective for Some Engines and Refrigerators* (Springer, New York, USA).

Ueda, Y., Yonemitsu, S., Ohashi, K., and Okamoto, T. (**2020**). "Measurement and Empirical Evaluation of Acoustic Loss in Tube with Abrupt Area Change," The Journal of the Acoustical Society of America **147**(1), 364–370.

Ward, B., Clark, J., and Swift, G. "Design Environment for Low-amplitude Thermoacoustic Energy Conversion DeltaEC Version 6.4b2.7 Users Guide" https://www.lanl.gov/org/ddste/aldps/materials-physics-applications/condensed-matter-magnet-science/thermoacoustics/computer-codes.php, accessed: 2023-03-06.

Weltsch, O., Offner, A., Liberzon, D., and Ramon, G. Z. (**2017**). "Adsorption-Mediated Mass Streaming in a Standing Acoustic Wave," Physical review letters **118**(24), 244301.